Alexandria Engineering Journal (2016) 55, 1025–1035

HOSTED BY

ELSEVIER

Alexandria University

Alexandria Engineering Journal

www.elsevier.com/locate/aej
www.sciencedirect.com

ORIGINAL ARTICLE

Unsteady Casson nanofluid flow over a stretching sheet with thermal radiation, convective and slip boundary conditions

Ibukun Sarah Oyelakin, Sabyasachi Mondal *, Precious Sibanda

School of Mathematics, Statistics and Computer Science, University of KwaZulu-Natal, Private Bag X01, Scottsville, Pietermaritzburg 3209, South Africa

Received 18 November 2015; revised 1 March 2016; accepted 3 March 2016
Available online 11 April 2016

KEYWORDS

Casson nanofluid;
Navier slip;
Soret and Dufour parameters;
Spectral relaxation method

Abstract In this paper we report on combined Dufour and Soret effects on the heat and mass transfer in a Casson nanofluid flow over an unsteady stretching sheet with thermal radiation and heat generation. The effects of partial slip on the velocity at the boundary, convective thermal boundary condition, Brownian and thermophoresis diffusion coefficients on the concentration boundary condition are investigated. The model equations are solved using the spectral relaxation method. The results indicate that the fluid flow, temperature and concentration profiles are significantly influenced by the fluid unsteadiness, the Casson parameter, magnetic parameter and the velocity slip. The effect of increasing the Casson parameter is to suppress the velocity and temperature growth. An increase in the Dufour parameter reduces the flow temperature, while an increase in the value of the Soret parameter causes increase in the concentration of the fluid. Again, increasing the velocity slip parameter reduces the velocity profile whereas increasing the heat generation parameter increases the temperature profile. A validation of the work is presented by comparing the current results with existing literature.

1. Introduction

The concept of nanofluids was introduced by Choi [1] where he proposed the suspension of nanoparticles in a base fluid such as water, oil, and ethylene glycol. Buongiorno [2] attempted to explain the increase in the thermal conductivity of such fluids and developed a model that took into account the particle Brownian motion and thermophoresis.

Noghrehabadi et al. [3] investigated the effects of the slip boundary condition on the heat transfer characteristics for a stretching sheet subjected to convective heat transfer in the presence of nanoparticles. They found that the flow velocity and the surface shear stress on the stretching sheet are strongly influenced by the slip parameter with a decrease in the momentum boundary layer thickness and increase in thermal boundary layer thickness. Khan and Pop [4] studied the problem of laminar fluid flow which results from a stretching of a flat surface in a nanofluid. They analyzed the development of the

* Corresponding author.
E-mail address: sabya.mondal.2007@gmail.com (S. Mondal).
Peer review under responsibility of Faculty of Engineering, Alexandria University.

http://dx.doi.org/10.1016/j.aej.2016.03.003

steady boundary layer flow, heat transfer and nanoparticle volume fraction over a stretching surface in the nanofluid. They observed that the reduced Nusselt number decreased while the reduced Sherwood number increased with the parameters considered in the study. They further obtained linear regression estimations in terms of Brownian and thermophoresis parameters for both the reduced Nusselt and Sherwood numbers. Nadeem et al. [5] studied two-dimensional boundary layer flow and heat transfer in steady incompressible Oldroyd-B nanofluid due to a stretching sheet. They showed that an increase in the Brownian motion parameter reduced the local Nusselt number while the local Sherwood number increased. Makinde et al. [6] studied the combined effects of buoyancy force, convective heating, Brownian motion, thermophoresis and a magnetic field on stagnation point flow and heat transfer due to a nanofluid flow from a stretching/shrinking sheet under the assumption that the magnetic Reynolds number was small. Their results showed that dual solutions exist for the shrinking case and an increase in the buoyancy force reduced both the skin friction coefficient and the local Sherwood number while the local Nusselt number increased. Haroun et al. [7] studied the heat and mass transfer in magnetohydrodynamic mixed convection flow of a nanofluid over an unsteady stretching/shrinking sheet. The flow considered was subject to a heat source and viscous dissipation. Soret and Dufour effects were assumed to be significant. They further assumed that the nanoparticle volume fraction at the wall could be actively controlled. The resulting fluid model equations were solved using the spectral relaxation method, an accurate technique for solving nonlinear boundary value problems. Recently, Haroun et al. [8] investigated magnetohydrodynamic nanofluid flow past an impulsively stretching surface with a chemical reaction and an applied magnetic field using the spectral relaxation method.

Casson fluid is classified as a non-Newtonian fluid due to its rheological characteristics in relation to the shear stress–strain relationship. It behaves like an elastic solid at low shear strain and above a critical stress value, it behaves like a Newtonian fluid. A Casson fluid can best be described as a shear thinning liquid with infinite viscosity at zero shear rate, and zero viscosity at an infinite rate of shear. Some common examples of liquids that exhibit Casson fluid characteristics include tomato sauce, honey, soup, orange juice and human blood.

Mustafa et al. [9] used the homotopy analysis method of solution to study the boundary layer flow of a Casson fluid near the stagnation-point on a stretching surface and presented results for the limiting case when the Casson parameter tends to infinity. Mustafa et al. [10] studied the momentum and thermal boundary layer development in a Casson fluid flow over a semi-infinite flat plate when both the ambient fluid and the flat plate are impulsively set in motion at the same time and the temperature of the flat plate is suddenly raised from that of the surrounding fluid. They derived parabolic partial differential equations which were solved analytically using the homotopy analysis method. Nandy [11] investigated the hydromagnetic boundary layer flow and heat transfer in a non-Newtonian Casson fluid with a stagnation point over a stretching surface in the presence of velocity and thermal slip boundary condition and the results indicated that the flow and temperature fields were greatly affected by the slip parameters on the velocity and thermal boundary conditions respectively. Makanda et al. [12] considered two-dimensional flow and diffusion of a chemically reactive species in Casson fluid from an unsteady stretching surface in the presence of magnetic field. It was generally noted that increasing the magnetic and permeability parameters reduced the velocity profiles, the coefficient of heat transfer and the concentration profiles while the skin friction increased. Bhattacharyya [13] considered two-dimensional magnetohydrodynamic stagnation point flow of an electrically conducting Casson fluid and heat transfer due to a stretching sheet under the effect of thermal radiation. They pointed out that the velocity boundary layer thickness for Casson fluid is larger than that of Newtonian fluids due to the plasticity of the Casson fluid. Mukhopadhyay et al. [14] studied Casson fluid flow over an unsteady stretching surface by extending the earlier work of Andersson et al. [15]. Hayat et al. [16] presented Soret and Dufour effects on two-dimensional flow of a Casson fluid induced by a stretching surface that is electrically conducting. They used the homotopy analysis method to solve the nonlinear system of ordinary differential equations. Nadeem [17] studied magnetohydrodynamic three dimensional Casson fluid flow past a porous linearly stretching sheet and they concluded that due to viscosity effects, the Newtonian fluid has less friction at the wall compared to the non-Newtonian fluid. Bhattacharyya [18] obtained analytical solutions for magnetohydrodynamic boundary layer flow of Casson fluid over a permeable stretching/shrinking sheet with wall mass transfer. Nadeem et al. [19] investigated the magnetohydrodynamic boundary layer flow of a Casson fluid over an exponentially permeable shrinking sheet. Nadeem et al. [20] discussed enhancement in the heat and mass transfer of a three dimensional magnetohydrodynamic Casson nanofluid and adjusted the hot fluid along the lower surface of the wall by introducing a convective boundary condition. They showed that a Newtonian nanofluid produces low skin friction at the wall compared to the Casson nanofluid and that there is low thermal conductivity for a higher Prandtl numbers. Mukhopadhyay [21] examined the effects of thermal radiation on Casson fluid flow and heat transfer over an unsteady stretching surface subjected to suction/blowing and they concluded that the Prandtl number can be used to increase the rate of cooling in the Casson fluid flow, temperature profile is intensified with increase in the radiation parameter, while the Casson parameter reduced the momentum boundary layer thickness and enhanced the thermal boundary layer thickness. Raju et al. [22] analyzed the flow, heat and mass transfer behavior of a Casson fluid past an exponentially permeable stretching surface in the presence of thermal radiation, a magnetic field, viscous dissipation, a heat source and chemical reaction, and they showed that increasing the heat source parameter reduced the temperature profiles in the boundary layer.

Recently, Kuznetsov and Nield [23] revisited their model on the natural convective boundary layer flow of a nanofluid over a vertical plate by including the effects of Brownian motion and thermophoresis. For the new model they argued that the nanofluid particle fraction at the boundary should be passively rather than actively controlled in order for the model to be physically realistic. This recent boundary condition provides one of the motivations for the present research.

The study of unsteady flow of Casson nanofluid has not been given much consideration so far. The aim of this paper is to study the fluid flow, heat and mass transfer in a Casson nanofluid, the Casson fluid being the base fluid. The

traditional Casson nanofluid model is revised to include the effect of thermophoresis and Brownian motion. In this paper we have studied the effects of various parameters (such as Soret, Dufour, thermal radiation, heat generation and unsteadiness parameters) on the fluid flow, heat and mass transfer profiles with Navier slip and thermal convective boundary conditions. The model equations are solved using the spectral relaxation method proposed by Motsa [24]. The spectral relaxation method has the characteristics of fast convergence and good accuracy as shown in some recent studies (see [25,26]). We give qualitative and quantitative comparisons with previously published work to show that our results are accurate.

2. Governing equations and boundary conditions

Consider the unsteady two-dimensional laminar flow and heat transfer of an incompressible Casson nanofluid past a stretching sheet with stretching velocity $u(x,t) = cx/(1-\lambda t)$, where $c > 0$, $\lambda \geqslant 0$ are constants and t is time. The unsteady stretching surface has a uniform temperature and nanoparticle concentration T_w and C_w respectively. The temperature and nanoparticle concentration far from the surface is T_∞ and C_∞ respectively.

The rheological equation of state for an isotropic and incompressible flow of a Casson fluid is expressed (see [11,29]) as:

$$\tau_{ij} = \begin{cases} 2\left(k_c + \frac{\tau_0}{\sqrt{2\pi}}\right)e_{ij} & \text{if } \pi > \pi_c \\ 2\left(k_c + \frac{\tau_0}{\sqrt{2\pi_c}}\right)e_{ij} & \text{if } \pi < \pi_c, \end{cases} \tag{1}$$

where

$$e_{ij} = \frac{1}{2}\left(\frac{\partial u_i}{\partial x_j} + \frac{\partial u_j}{\partial x_i}\right), \tag{2}$$

is the rate of strain tensor, τ_{ij} is the component of stress tensor, k_c is the Casson coefficient of viscosity, $\pi = e_{ij}e_{ij}$ is the product of the rate of strain tensor with itself, π_c is the critical value of the product of the rate of strain tensor with itself, τ_0 is the yield stress of the fluid and u_i are the velocity components. It is assumed that both temperature and concentration at the surface vary with distance and time from the origin, thus the temperature T_w and concentration C_w at the surface are given by:

$$T_w(x,t) = T_\infty + \frac{bx^2}{(1-\lambda t)^2}, \quad C_w(x,t) = C_\infty + \frac{b_1 x^2}{(1-\lambda t)^2} \tag{3}$$

where b and b_1 are constants. It should be noted that the expressions $u_w(x,t)$, $T_w(x,t)$, and $C_w(x,t)$ are valid only for time $t < \lambda^{-1}$, but not when $\lambda = 0$.

Table 1 The values of $f''(0)$ for various values of unsteadiness parameter A for Newtonian fluid.

A	Present results	Sharidan et al. [28]	Chamka et al. [29]	Mukhopadhyay et al. [14]
0.8	−1.261043	−1.261042	−1.261512	−1.261479
1.2	−1.377725	−1.377722	−1.378052	−1.377850

Table 2 Comparison of values of $f''(0)$ with those of existing literature for various values of α when $\beta \to \infty$.

α	Present	Mustafa et al. [9]	Mahapatra and Gupta [30]	Ishak et al. [31]
0.01	−0.99782	−0.99802	–	−0.9980
0.10	−0.96937	−0.96939	−0.9694	−0.9694
0.20	−0.918111	0.918107	0.9181	0.9181
0.50	−0.66726	−0.66735	−0.6673	−0.6673
2.00	2.01750	2.01757	2.0175	2.0175
3.00	4.72928	4.72964	4.7294	4.7294

Table 3 Comparison of values for skin friction coefficient for various values of β and M with those of Nadeem et al. [19] when $\alpha = 0$.

β	M	Present	Nadeem et al. [19]
∞	0	1.00000	1.0042
5		−1.09544	−1.0954
1		−1.41421	−1.4142
∞	10	−3.31662	−3.3165
5		−3.63318	−3.6331
1		−4.69042	−4.6904
∞	100	−10.04987	−10.049
5		−11.00909	−11.0091
1		−14.21267	−14.2127

The continuity, momentum, energy and concentration equations of the unsteady incompressible Casson nanofluid boundary layer flow are as follows (see [11]):

$$\frac{\partial u}{\partial x} + \frac{\partial v}{\partial y} = 0, \tag{4}$$

$$\frac{\partial u}{\partial t} + u\frac{\partial u}{\partial x} + v\frac{\partial u}{\partial y} = U\frac{dU}{dx} + \nu\left(1+\frac{1}{\beta}\right)\frac{\partial^2 u}{\partial y^2} + \frac{\sigma B_0^2}{\rho}(U-u), \tag{5}$$

$$\begin{aligned}\frac{\partial T}{\partial t} + u\frac{\partial T}{\partial x} + v\frac{\partial T}{\partial y} &= \frac{k_0}{\rho c_p}\frac{\partial^2 u}{\partial y^2} + \frac{\nu}{c_p}\left(1+\frac{1}{\beta}\right)\left(\frac{\partial u}{\partial y}\right)^2 + \frac{\sigma B_0^2}{\rho}(U-u)^2 \\ &- \frac{1}{\rho c_p}\frac{\partial q_r}{\partial y} + \frac{Q_0}{\rho c_p}(T-T_\infty) + \tau\left[D_B\frac{\partial C}{\partial y}\frac{\partial T}{\partial y} + \frac{D_T}{T_\infty}\left(\frac{\partial T}{\partial y}\right)^2\right] \\ &+ \frac{D_m k_0}{c_s c_p}\frac{\partial^2 C}{\partial y^2},\end{aligned} \tag{6}$$

$$\frac{\partial C}{\partial t} + u\frac{\partial C}{\partial x} + v\frac{\partial C}{\partial y} = D_B\frac{\partial^2 C}{\partial y^2} + \frac{D_T}{T_\infty}\frac{\partial^2 T}{\partial y^2} + \frac{D_m k_0}{T_m}\frac{\partial^2 T}{\partial y^2}, \tag{7}$$

where u and v are the velocity components along the x- and y-directions, respectively, ν is the kinematic Casson fluid viscosity, ρ is the density of the fluid, σ is the electrical conductivity, B_0 is the uniform magnetic field along y-axis, c_p is the specific heat at constant pressure and $\beta = k_c\sqrt{2\pi_c}/\tau_0$ is the non-Newtonian Casson parameter. k_0 is the thermal diffusivity, q_r is the radiation heat flux, Q_0 is the heat generation constant, $\tau = (\rho c)_p/(\rho c)_f$ is the ratio of the heat capacity of the nanoparticle material and the heat capacity of the fluid, D_B is the Brownian diffusion coefficient, D_T is the

Table 4 Comparison of results for $-f''(0)$ with the slip factor δ.

δ	Present results	Noghrehabadi et al. [3]	Sahoo and Do [32]
0	1.000000	1.0	1.001154
0.1	0.872083	0.872082	0.871447
0.2	0.776377	0.776377	0.774933
0.3	0.701548	0.701548	0.699738
0.5	0.591195	0.591195	0.589195
1.0	0.430160	0.430160	0.428450
2.0	0.283979	0.283980	0.282893
3.0	0.214054	0.214055	0.213314
5.0	0.144714	0.144841	0.144430
10	0.080932	0.081243	0.081091
20	0.043569	0.043790	0.043748

thermophoretic diffusion coefficient, D_m is the mass diffusivity, c_s is the concentration susceptibility, and T_m is the mean temperature.

The dimensional boundary conditions are:

$$u = u_w(x,t) + u_{slip}(x,t), \qquad v = 0, \qquad -k^* \frac{\partial T}{\partial y} = h_f(T_w - T),$$
$$D_B \frac{\partial C}{\partial y} + \frac{D_T}{T_\infty}\frac{\partial T}{\partial y} = 0 \qquad \text{at} \qquad y = 0, \tag{8}$$
$$u \to U(x,t) = \frac{ax}{1-\lambda t}, \frac{\partial u}{\partial y} \to 0, \quad T \to T_\infty,$$
$$C \to C_\infty \quad \text{as} \quad y \to \infty, \tag{9}$$

where

$$u_w(x,t) = \frac{cx}{1-\lambda t}, \quad u_{slip}(x,t) = Lv\frac{\partial u}{\partial y} \quad \text{and} \quad L = N(1-\lambda t)^{\frac{1}{2}}, \tag{10}$$

is the slip velocity factor, $k^* = k_0(1-\lambda t)^{\frac{1}{2}}$ is the thermal conductivity and h_f is the convective heat transfer coefficient.

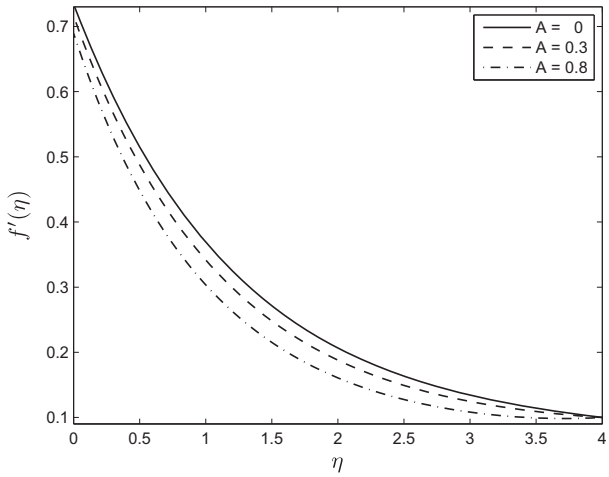

Figure 1 Effect of the unsteadiness parameter A on the velocity profile $f'(\eta)$ when $\delta = Bi = 0.5, Ec = 0.1, \alpha = 0.1, N_R = Nb = Nt = 0.5$, $He = 0.3, Df = 0.5, \beta = 1.0, M = 0.5, Pr = 1.0, Sr = 1.0$ and $Sc = 1.0$.

We introduce the stream function ψ defined in the usual way in terms of the velocity components, a similarity variable η and the following similarity transformations;

$$\eta = \sqrt{\frac{c}{v(1-\lambda t)}}, \quad \psi = \sqrt{\frac{cv}{(1-\lambda t)}} x f(\eta),$$
$$T_w = T_\infty + \frac{bx^2}{(1-\lambda t)^2}\theta(\eta), \quad C_w = C_\infty + \frac{b_1 x^2}{(1-\lambda t)^2}\phi(\eta). \tag{11}$$

where $f(\eta), \theta(\eta)$ and $\phi(\eta)$ are the non-dimensional velocity, temperature and concentration respectively. Substituting into Eqs. (4)–(7), gives the non-dimensional equations;

$$\left(1+\frac{1}{\beta}\right)f''' + ff'' - f'^2 - A\left(f' + \frac{\eta}{2}f''\right) + \alpha^2 + M(\alpha - f') = 0, \tag{12}$$

Table 5 Computed values of Skin friction coefficient, heat transfer coefficient and mass transfer coefficient when $A = 0.8$, $Bi = 0.5$, $Pr = Sc = 1$, $Nt = 0.5$, $Nb = 0.3$, $He = 0.3$, $Ec = 0.3$, $\alpha = 0.2$ and $\delta = 0.1$ for different values of β, M, Df, Sr and N_R.

β	M	Df	Sr	N_R	$(1+\frac{1}{\beta})f''(0)$	$-\theta'(0)$	$-\phi'(0)$
0.5					−3.23231	−0.31768	0.52947
1.0	5.0	0.5	0.4	0.2	−2.56075	−0.33313	0.55522
2.0					−2.16359	−0.34371	0.57284
	0.5				−1.44319	−0.40475	0.67458
2.0	1.0	0.5	0.4	0.2	−1.54818	−0.39609	0.66014
	2.0				−1.73352	−0.38055	0.63425
		0.0			−2.16359	−0.31031	0.51718
2.0	5.0	0.1	0.4	0.2	−2.16359	−0.31658	0.52763
		0.3			−2.16359	−0.33020	0.55034
			0.1		−2.16359	−0.34587	0.57644
2.0	5.0	0.5	0.5	0.2	−2.16359	−0.34227	0.57044
			0.7		−2.16359	−0.33490	0.55817
				0.5	−2.16359	−0.33718	0.56197
2.0	5.0	0.5	0.4	1.0	−2.16359	−0.32389	0.53982
				3.0	−2.16359	−0.28473	0.47456

$$\frac{1}{Pr}(1+N_R)\theta'' - A\left(2\theta+\frac{\eta}{2}\theta'\right) - 2f'\theta + f\theta' + He\theta + Nt\theta'^2 + Nb\theta'\phi' + \left(1+\frac{1}{\beta}\right)Ecf''^2 + MEc(\alpha - f')^2 + Df\phi'' = 0, \quad (13)$$

$$\phi'' - Sc\left[A(2\phi+\frac{\eta}{2}\phi') + 2f'\phi - f\phi' - Sr\theta''\right] + \frac{Nt}{Nb}\theta'' = 0, \quad (14)$$

subject to the boundary conditions

$$f(0)=0, \quad f'(0)=1+\delta f''(0), \quad f'(\infty)=\alpha, \quad f''(\infty)=0, \quad (15)$$

$$\theta'(0) = -Bi(1-\theta(0)), \quad \theta(\infty)=0, \quad (16)$$

$$Nb\phi'(0) + Nt\theta'(0) = 0, \quad \phi(\infty)=0, \quad (17)$$

where differentiation is with respect to η and $A=\lambda/c$ is the unsteadiness parameter, $\alpha = a/c$ is the dimensionless velocity ratio parameter, $M = \frac{\sigma B^2}{c\rho}$ is the magnetic parameter, $Pr = \nu\rho c_p/k_0$ is the Prandtl number, $Sc = \nu/D_B$ is the Schmidt number, $He = Q/c\,\rho c_p$ is the heat generation parameter, $Nb = \tau D_B(C_w - C_\infty)/\nu$ is the Brownian motion parameter, $Nt = \tau D_T(T_w - T_\infty)/\nu T_\infty$ is the thermophoresis parameter, $Df = \frac{D_m k_0(C_w - C_\infty)}{c_s c_p \nu(T_w - T_\infty)}$ is the Dufour number, $N_R = \frac{16\sigma^* T_\infty^3}{3k^*\nu\rho c_p k_0}$ is the radiation parameter, $Ec = c^2/bc_p$ is the Eckert number, $Sr = \frac{D_m k_0(T_w - T_\infty)}{T_m \nu(C_w - C_\infty)}$ is the Soret number, $\delta = N\sqrt{c\nu}$ is the dimensionless velocity slip parameter and $Bi = \sqrt{\nu/c}\,h_f/k_0$ is the Biot number.

3. Method of solution

In this section, the spectral relaxation method (SRM) is used to solve the nonlinear differential Eqs. (12)–(14). The SRM algorithm (see [24–26]) first decouples the system of equations and an iteration scheme is then developed from the decoupled equations by evaluating linear terms at the current iteration level $r+1$. To use this method, we first reduce the order of the equations as follows;

$$f'_{r+1} = g_r, \quad f_{r+1}(0)=0, \quad (18)$$

$$\left(1+\frac{1}{\beta}\right)g''_{r+1} + \left(f_{r+1} - A\frac{\eta}{2}\right)g'_{r+1} - (A+M)g_{r+1} = g_r^2 - \alpha^2 - M\alpha, \quad (19)$$

$$\frac{1}{Pr}(1+N_R)\theta''_{r+1} + \left(f_{r+1} - A\frac{\eta}{2} + Nb\phi'_r\right)\theta'_{r+1} - 2g_{r+1}\theta_{r+1} - (2A - He)\theta_{r+1} = -Nt\theta'^2_r - \left(1+\frac{1}{\beta}\right)Ecg'^2_{r+1} - MEc(\alpha - g_{r+1})^2 - Df\phi''_r, \quad (20)$$

$$\phi''_{r+1} + Sc\left(f_{r+1} - A\frac{\eta}{2}\right)\phi'_{r+1} - 2Scg_{r+1}\phi_{r+1} - 2ASc\phi_{r+1} = -(SrSc + Nt/Nb)\theta''_{r+1}, \quad (21)$$

subject to

$$g_{r+1}(0) = 1 + \delta g'_{r+1}(0), \qquad g_{r+1}(\infty)=\alpha, \quad g'_{r+1}(\infty)=0, \quad (22)$$

$$\theta'_{r+1}(0) = -Bi(1-\theta_{r+1}(0)), \quad \theta_{r+1}(\infty)=0,$$
$$Nb\phi'_{r+1}(0) + Nt\theta'_{r+1}(0) = 0, \phi_{r+1}(\infty)=0. \quad (23)$$

Eqs. (18)–(22) are solved using the Chebyshev pseudo-spectral method [24]. The unknown functions are defined by Chebyshev interpolating polynomials with Gauss–Lobatto points defined by

$$\xi_i = \cos\frac{\pi i}{N}, \quad i=0,1,\ldots,N; \quad -1 \leqslant \xi \leq 1, \quad (24)$$

where N is the number of collocation points used. The semi-infinite domain is approximated by the truncated domain $[0, L]$ for convenience of numerical computations. Using the linear transformation $\eta = L(\xi+1)/2$, the interval $[0, L]$ is transformed into the interval $[-1, 1]$, where L is a scaled parameter used as the boundary condition value at infinity. It is a large but finite number chosen to represent the behavior of the flow properties when η is very large.

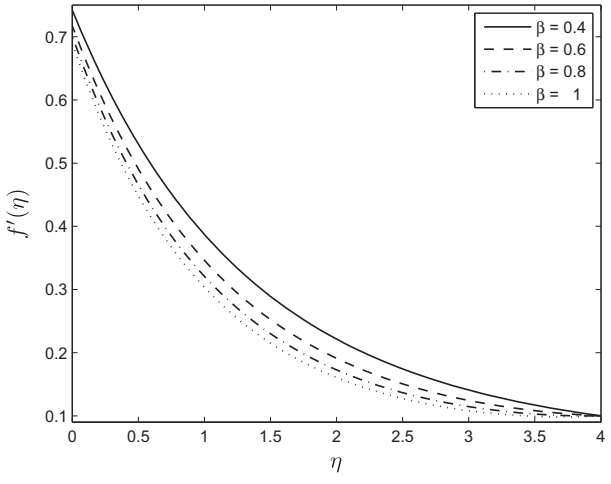

Figure 2 Effect of the Casson parameter β on the velocity profile $f'(\eta)$ when $\delta = Bi = 0.5, \alpha = 0.1, N_R = Nb = Nt = 0.5, He = 0.3, Df = 0.5, Sr = 1.0, \quad M = 0.5, Sc = 1.0, Ec = 1.0, Pr = 1.0$ and $A = 0.8$.

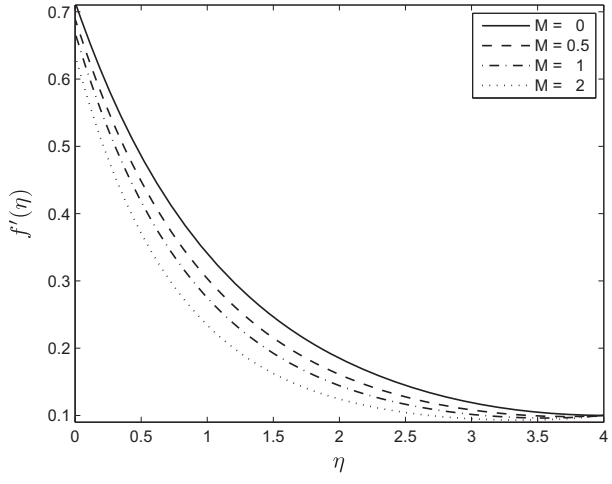

Figure 3 Effect of the magnetic parameter M on the velocity profile $f'(\eta)$ when $\delta = Bi = 0.5, \alpha = 0.1, N_R = Nb = Nt = 0.5, He = 0.3, Ec = 0.1, Df = 0.5, Sr = 1, Pr = 1, Sc = \beta = 1.0$ and $A = 0.8$.

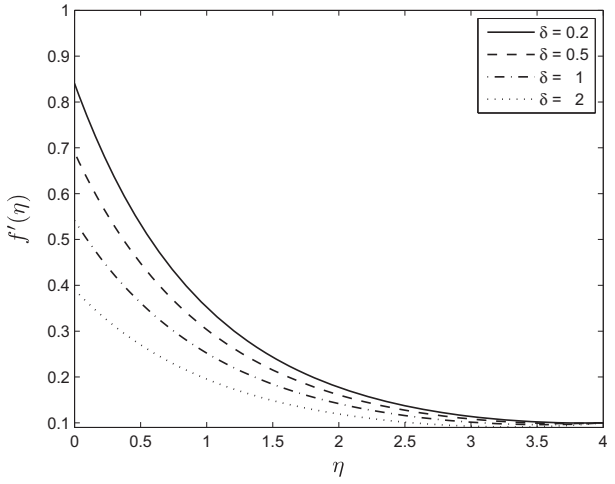

Figure 4 Effect of the velocity slip parameter δ on the velocity profile $f'(\eta)$ when $Bi = 0.5, \alpha = 0.1, N_R = 0.5, Nb = Nt = 0.5, He = 0.3, Ec = 0.1, Df = 0.5, Sr = 1.0, M = 0.5, Pr = 1.0, Sc = 1.0, \beta = 1.0$ and $A = 0.8$

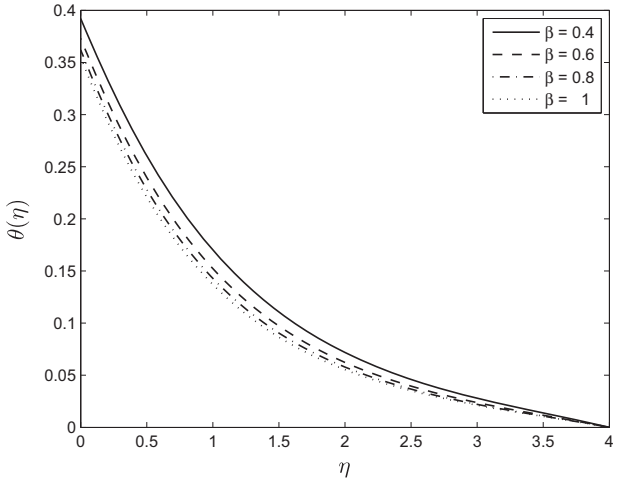

Figure 5 Effect of the Casson parameter β on the temperature profile $\theta(\eta)$ when $\alpha = 0.1, \delta = Bi = 0.5, N_R = Nb = Nt = 0.5, He = 0.3, Ec = 1.0, Df = 0.5, Sr = 1.0, M = 0.5, Pr = Sc = 1.0$ and $A = 0.8$.

The differentiation matrix $\mathbf{D}$ used to approximate the derivatives of the unknown variables is defined by:

$$\frac{df}{d\eta} = \Sigma_{k=0}^{N} \mathbf{D}_{ik} f(\xi_k) = \mathbf{D}f, \quad i = 1, 2, \ldots, N, \tag{25}$$

where $\mathbf{D} = 2D/L$ and $f = [f(\xi_0), f(\xi_1), \ldots, f(\xi_N)]^T$ is the vector function at the collocation points. Discretizing Eqs. (18)–(22) using the spectral relaxation method, we obtain the following matrix equations:

$$\mathbf{A_1 f_{r+1}} = \mathbf{B_1}, \quad f_{r+1}(\xi_N) = 0, \tag{26}$$

$$\mathbf{A_2 g_{r+1}} = \mathbf{B_2}, \quad g_{r+1}(\xi_N) = 1 + \delta g'_{r+1}(\xi_N), \quad g_{r+1}(\xi_0) = \alpha, \quad g'_{r+1}(\xi_0) = 0, \tag{27}$$

$$\mathbf{A_3 \Theta_{r+1}} = \mathbf{B_3}, \quad \theta'_{r+1}(\xi_N) = -Bi(1 - \theta_{r+1}(\xi_N)), \quad \theta_{r+1}(\xi_0) = 0, \tag{28}$$

$$\mathbf{A_4 \Phi_{r+1}} = \mathbf{B_4}, \quad Nb\phi'_{r+1}(\xi_N) + Nt\theta'_{r+1}(\xi_N) = 0, \quad \phi_{r+1}(\xi_0) = 0, \tag{29}$$

where

$$\mathbf{A_1} = \mathbf{D}, \quad \mathbf{B_1} = \mathbf{g_r} \tag{30}$$

$$\mathbf{A_2} = \left(1 + \frac{1}{\beta}\right)\mathbf{D}^2 + \mathrm{diag}\left[\mathbf{f_{r+1}} - A\frac{\eta}{2}\right]\mathbf{D} - (A + M)\mathbf{I},$$

$$\mathbf{B_2} = \mathbf{g_r^2} - \alpha^2 - M\alpha, \tag{31}$$

$$\mathbf{A_3} = \frac{1}{Pr}(1 + N_R)\mathbf{D}^2 + \mathrm{diag}\left[\mathbf{f_{r+1}} - A\frac{\eta}{2} + Nb\mathbf{\Phi'_r}\right]\mathbf{D} - 2\mathrm{diag}\left[\mathbf{g_{r+1}}\right] - (2A - He)\mathbf{I}, \tag{32}$$

$$\mathbf{B_3} = -Nt\boldsymbol{\theta}'^2_{\mathbf{r}} - \left(1 + \frac{1}{\beta}\right)Ec\mathbf{g'^2_{r+1}} - MEc(\alpha - \mathbf{g_{r+1}})^2 - Df\mathbf{\Phi'_r}, \tag{33}$$

$$\mathbf{A_4} = \mathbf{D}^2 + Sc\mathrm{diag}\left[\mathbf{f_{r+1}} - A\frac{\eta}{2}\right]\mathbf{D} - 2Sc\mathrm{diag}\left[\mathbf{g_{r+1}}\right] - 2ASc\mathbf{I}, \tag{34}$$

$$\mathbf{B_4} = -(SrSc + Nt/Nb)\mathbf{\Theta''_{r+1}}. \tag{35}$$

Here I is an $(N + 1) \times (N + 1)$ identity matrix, *diag*[] denotes a diagonal matrix and $\mathbf{f}$, $\mathbf{g}$, $\mathbf{\Theta}$, and $\mathbf{\Phi}$ are the values of functions f, g, θ and ϕ respectively when evaluated at the collocation points. The matrix systems (26)–(29) constitute the SRM scheme in which the equations are solved iteratively starting with suitable initial guesses $f_0(\eta)$, $g_0(\eta)$, $\theta_0(\eta)$ and $\phi_0(\eta)$.

4. Results and discussion

In this study the governing equations were solved using the spectral relaxation method. Extensive calculations were performed to obtain the velocity, temperature, concentration profiles as well as the skin friction, the local Nusselt number and the local Sherwood number for various physical parameters values. Tables 1 to 4 give a comparison of the skin friction coefficient with the previously published results. Table 1 shows the skin friction coefficient for various values of the unsteadiness parameter A for a Newtonian fluid (i.e., when $\beta \to \infty$)

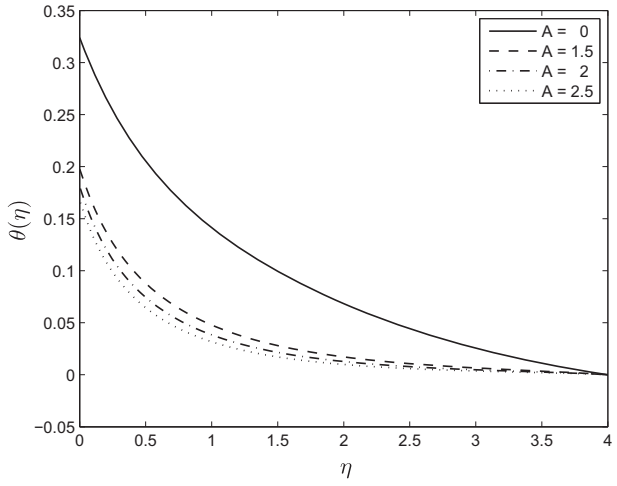

Figure 6 Effect of the unsteadiness parameter A on the temperature profile $\theta(\eta)$ when $\delta = Bi = 0.5, N_R = Nb = Nt = 0.5, He = 0.3, Ec = 0.1, Df = 0.5, Sr = 1.0, M = 0.5, Pr = 1.0, Sc = 1.0, \beta = 1.0$ and $\alpha = 0.1$.

which is compared with previously published results [14,28,29] when the other parameter values remain same. Table 2 displays the skin friction coefficient for various values of α when $\beta \to \infty$ which are compared with previously published results [9,30,31] when the other parameter values remain unchanged. Table 3 depicts the skin friction coefficient for various values of β and M and compares these values with those of Nadeem et al. [19] when $\alpha = 0$ and other parameters are remain unchanged. Table 4 shows the skin friction coefficient for various values of δ when compared with results in Noghrehabadi et al. [3] and Sahoo and Do [32]. It is seen that a very good agreement with the previously published results is achieved thus validating the accuracy of the current numerical results.

Table 5 displays the computed values of the skin friction coefficient, the heat transfer coefficient and the mass transfer coefficient when $A = 0.8$, $Bi = 0.5$, $Pr = Sc = 1$, $Nt = 0.5$, $Nb = 0.3$, $He = 0.3$, $Ec = 0.3$, $\alpha = 0.2$ and $\delta = 0.1$, for different values of β, M, Df, Sr and N_R. We note that an increase in β increases the skin-friction coefficient whereas increasing M reduces the skin-friction coefficient. The local Nusselt number is reduced by increasing β and Df while the local Sherwood number increases when β and Df are increased, whereas local Nusselt number increases by increasing M but the opposite trend is observed in case of the local Sherwood number. Again, the local Nusselt number increases and local Sherwood number decreases when increasing the values of Sr and N_R.

Fig. 1 shows the effect of the unsteadiness parameter on the velocity profiles. Here, it is shown that increasing the unsteadiness parameter reduces the velocity profiles. The velocity along the sheet decreases with an increase in the unsteadiness parameter due to the accompanying reduction in the thickness of the momentum boundary layer. Similar flow patterns for Casson fluid can be found in the literature, for instance, see [14,21].

Fig. 2 shows the effect of the Casson parameter β on the velocity profiles. We note that as β increases, the velocity and the boundary layer thickness decrease. Hence, the magnitude of the velocity is greater in Casson fluid when compared with viscous fluids. Nandy [11,18,21] investigated similar patterns of fluid flow.

Fig. 3 shows the effect of the magnetic parameter M on velocity profiles f'. The velocity profiles decrease with increasing magnetic field parameter values leading to a reduction in the velocity boundary layer thickness. The Lorentz force which opposes the motion occurs due to the applied transverse magnetic field, and is responsible for reducing the fluid velocity. Similar type of fluid flow patterns have been observed in [11,18].

Fig. 4 shows that the velocity profiles are decreasing function of the slip parameter δ. This implies that when slip occurs (for non-zero values of δ) the fluid velocity near the sheet is no longer equal to the stretching sheet velocity. Increasing δ decreases the velocity because under the slip condition, the pulling of the stretching sheet can be only partly transmitted to the fluid. The boundary layer thickness also decreases as the slip parameter δ increases.

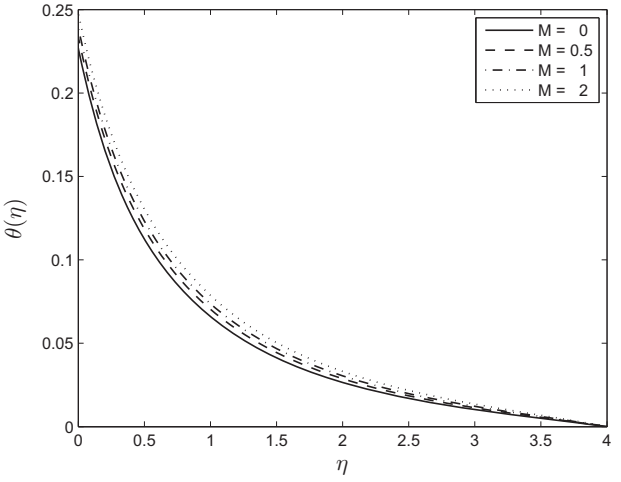

Figure 8 Effect of the magnetic parameter M on the temperature profile $\theta(\eta)$ when $\delta = 0.5, Bi = 0.5, N_R = Nb = Nt = 0.5, He = 0.3, Ec = 0.1, Df = 0.5, Sr = 1.0, Pr = 1.0, Sc = 1.0, \alpha = 0.1, \beta = 1.0$ and $A = 0.8$.

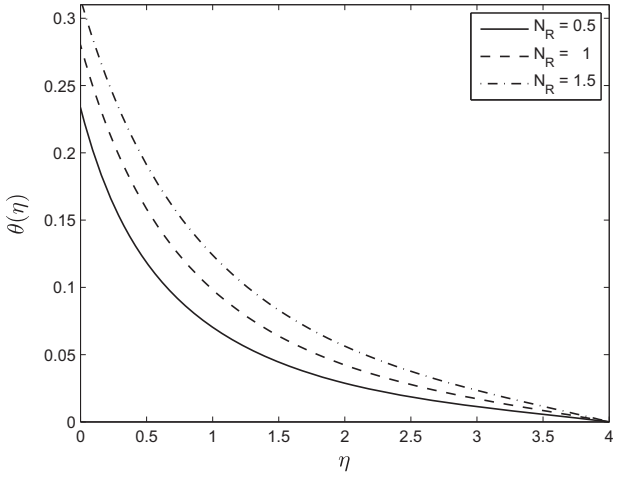

Figure 7 Effect of the thermal radiation parameter N_R on the temperature profile $\theta(\eta)$ when $\delta = 0.5, Bi = 0.5, Nb = Nt = 0.5, He = 0.3, Ec = 0.1, Df = 0.5, Sr = 1.0, M = 0.5, Pr = 1.0, Sc = 1.0, \alpha = 0.1, \beta = 1.0$ and $A = 0.8$.

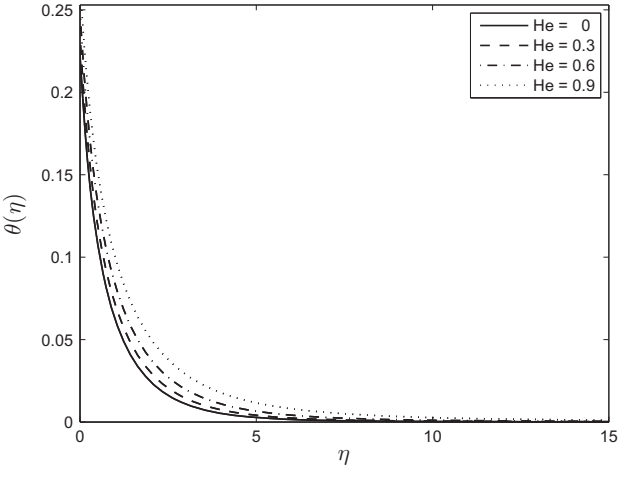

Figure 9 Effect of the heat generation parameter He on the temperature profile $\theta(\eta)$ when $\alpha = 0.1, \delta = 0.5, Bi = 0.5, N_R = Nb = Nt = 0.5, Sr = 1.0, Ec = 0.1, Df = 0.5, M = 0.5, Pr = 1.0, Sc = 1.0, \beta = 1.0$ and $A = 0.8$.

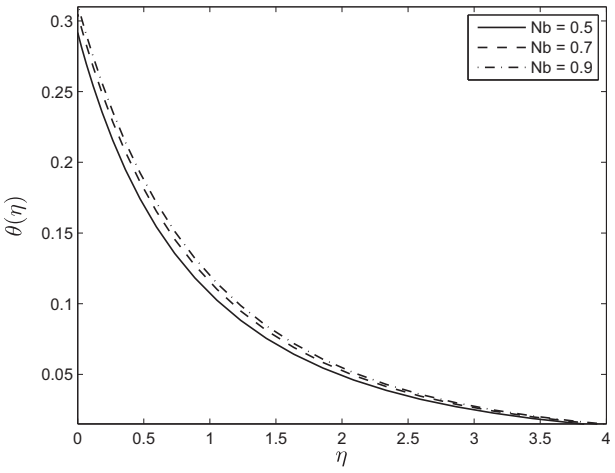

Figure 10 Effect of the Brownian motion parameter Nb on the temperature profile $\theta(\eta)$ when $\alpha = 0.1, \delta = Bi = 0.5, N_R = 0.5, Nt = 0.5, He = 0.3, Ec = 0.1, Df = 0.5, Sr = 1.0, M = 0.5, Pr = 0.7, Sc = 1.0, \beta = 1.0$ and $A = 0.8$.

Fig. 5 shows that the temperature profiles decrease with increasing the value of the Casson parameters β. Increasing the Casson parameter, i.e., reducing the yield stress suppresses the fluid velocity. The temperature curves in Fig. 5 show that the rate of transport is considerably reduced by an increase in β.

Fig. 6 shows that the temperature profiles decrease significantly as the unsteadiness parameter increases. The rate of heat transfer (from the sheet to the fluid) decreases with increasing values of A. Less heat is transferred from the sheet to the fluid when the unsteadiness parameter increases. For this reason the temperature profiles $\theta(\eta)$ decrease. Since the fluid flow is caused solely by the stretching sheet and the sheet surface temperature is higher than the free stream temperature, the fluid velocity and temperature decrease as A increases. It is important to note that the rate of cooling is much faster for higher values of unsteadiness parameter. In the studies [14,21] similar temperature profiles patterns were obtained.

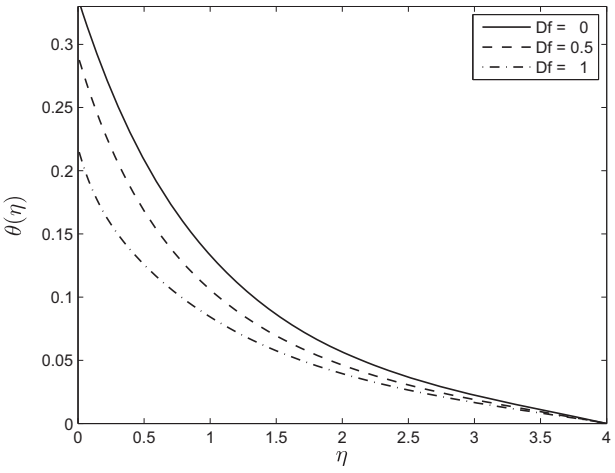

Figure 11 Effect of the Dufour number Df on the temperature profile $\theta(\eta)$ when $\alpha = 0.1, \delta = Bi = 0.5, N_R = 0.5, Nt = 0.5, He = 0.3, Ec = 0.1, Nb = 0.5, Sr = 1.0, M = 0.5, Pr = 0.7, Sc = 1.0, \beta = 1.0$ and $A = 0.8$.

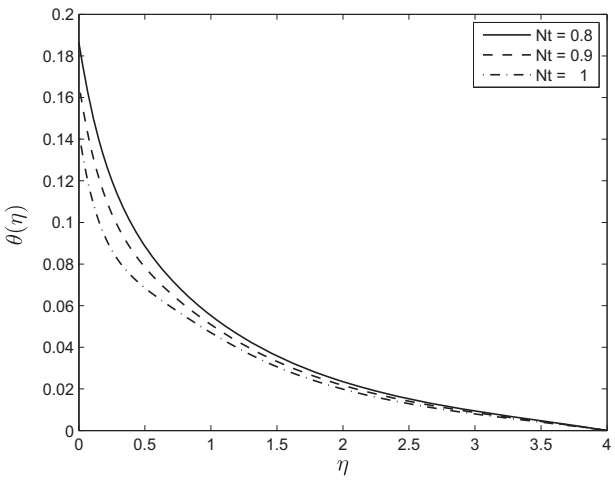

Figure 12 Effect of the thermophoresis parameter Nt on the temperature profile $\theta(\eta)$ when $\alpha = 0.1, \delta = 0.5, Bi = 0.5, N_R = Nb = 0.5, He = 0.3, Ec = 0.1, Df = 0.5, M = 0.5, Pr = 1.0, Sc = Sr = 1.0, \beta = 1.0$ and $A = 0.8$.

Fig. 7 shows that the temperature profiles increase as thermal radiation increases, and because the effect of N_R is to enhance heat transfer, the thermal boundary layer thickness increases with thermal radiation.

Fig. 8 shows that magnetic field increases the temperature profiles. Because of the application of transverse magnetic field in an electrically conducting fluid. It is also noticed that the thermal boundary layer thickness increases in the presence of a magnetic field. Fig. 9 shows that increasing heat generation parameter enhances the temperature profiles thereby increasing the thermal boundary layer thickness. Fig. 10 shows that temperature profiles increase with increasing the Brownian motion parameter. Because of this increase in the temperature profiles, there is also an enhancement in the thermal boundary layer thickness.

Fig. 11 shows the effect of the Dufour number on the temperature profiles. Increasing Df parameter leads to a decrease

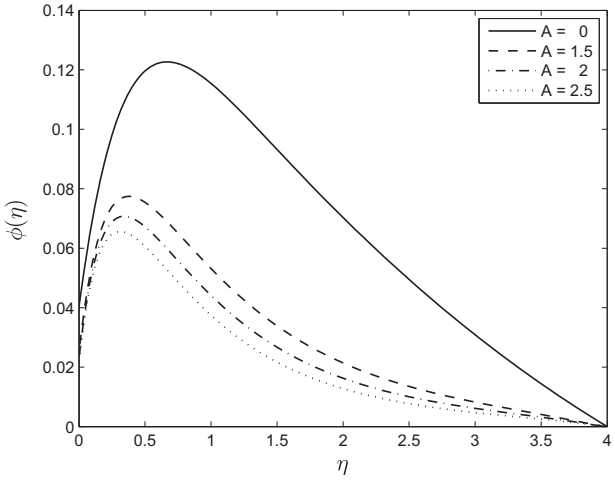

Figure 13 Effect of the unsteadiness parameter A on the concentration profile $\phi(\eta)$ when $\alpha = 0.1, \delta = 0.5, Bi = 0.5, N_R = Nb = Nt = 0.5, He = 0.3, Ec = 0.1, Df = 0.5, M = 0.5, Pr = 1.0, Sc = Sr = 1.0$ and $\beta = 1.0$.

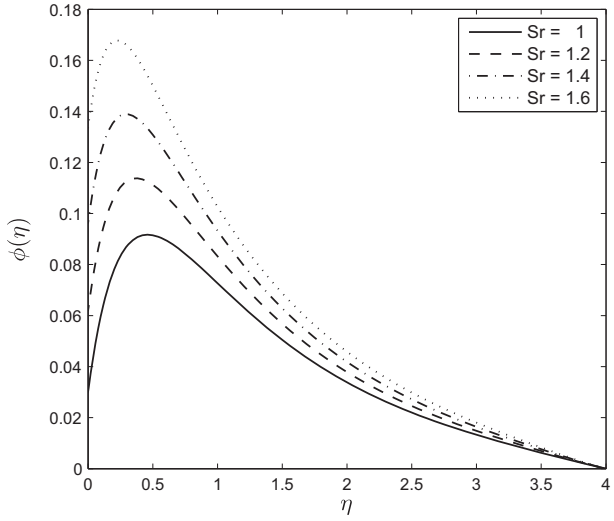

Figure 14 Effect of the Soret number Sr on the concentration profile $\phi(\eta)$ when $\alpha = 0.1, \delta = 0.5, Bi = 0.5, N_R = Nb = Nt = 0.5, He = 0.3, Ec = 0.1, Df = 0.5, M = 0.5, Pr = 1.0, Sc = 1.0, \beta = 1.0$ and $A = 0.8$.

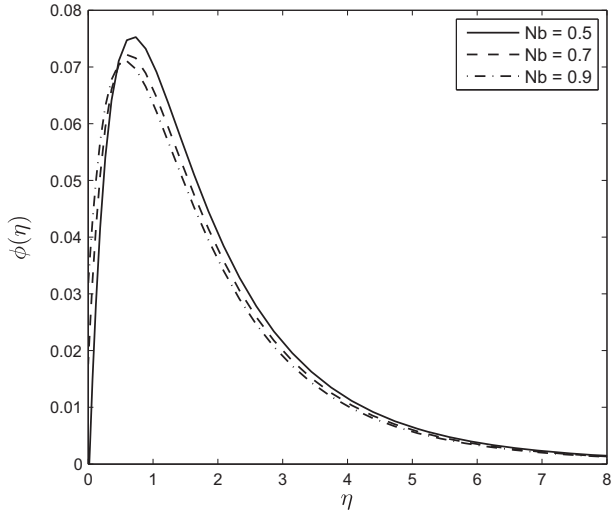

Figure 15 Effect of the Brownian motion parameter Nb on the concentration profile $\phi(\eta)$ when $\alpha = 0.1, \delta = Bi = 0.5, N_R = 0.5, Nt = 0.5, He = 0.3, Ec = 0.1, Df = 0.5, Sr = 1.0, M = 0.5, Pr = 0.7, Sc = 1.0, \beta = 1.0$ and $A = 0.8$.

in the temperature profiles. Dufour effect is the heat transfer induced by volume fraction gradients and significant because of the density difference in the flow regime. Thus the figure shows the effect of the concentration gradient on the thermal energy flux in the flow region. Since it is decreasing, it implies that the effect of the composition gradient on temperature is reduced and this leads to a cooling of the boundary layer region, as explained in [33]. Effect of the thermophoresis is given in Fig. 12. From the figure, it is observed that the temperature profiles are decreased as the thermophoresis parameter is increasing and due to this effect, the thermal boundary layer thickness is also decreased. Fig. 13 shows that the concentration profiles decrease with increasing values of A. As can be observed in Figs. 1, 6 and 13, increasing value of the unsteadiness parameter A reduces the flow properties such as velocity, temperature and concentration. When A values are increased in the system, the boundary layer thicknesses are reduced and this inhibits the development of transition from laminar to turbulent flow. This shows that stretching of surfaces can be used as a flow stabilizing mechanism. Fig. 14 shows that the concentration boundary layer thickness increases with Sr and consequently, leads to an increase in the concentration profiles due to enhancement of the profiles by the mass flux created by the temperature gradient. This similar trend is observed with some other fluid types like micropolar fluids as pointed out in [33,34]. Fig. 15 shows that increasing the values of the Brownian motion parameter first causes a sharp decrease in the concentration profiles followed by a slight increase. The concentration profiles decrease with increasing Nb near the stretching sheet wall up to a certain value of η but beyond this point, the opposite trend is observed. Near the wall the concentration boundary layer decreases with increasing Nb but away from the wall, we observe the opposite trend. Fig. 16 shows the influence of the thermophoresis parameter on the concentration profiles. It is seen from this figure that the concentration profiles increase with increasing Nt near the stretching sheet wall

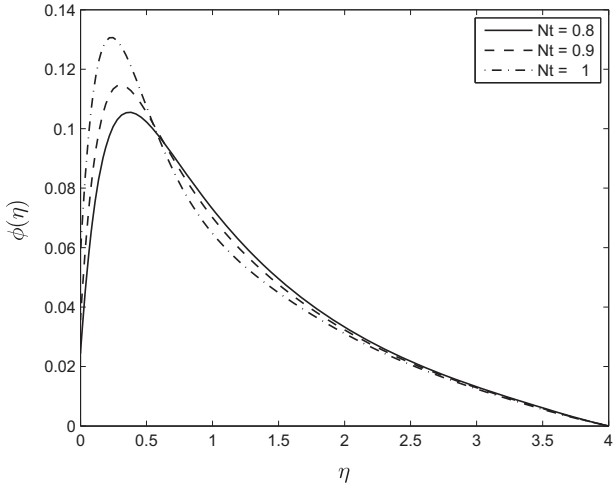

Figure 16 Effect of the thermophoresis parameter Nt on the concentration profile $\phi(\eta)$ when $\alpha = 0.1, \delta = Bi = 0.5, N_R = Nb = 0.5, He = 0.3, Ec = 0.1, Df = 0.5, Sr = 1.0, M = 0.5, Pr = 1.0, Sc = 1.0, \beta = 1.0$ and $A = 0.8$.

up-to a certain value of η but beyond this point, the opposite trend is observed. It means that concentration boundary layer thickness increases up-to a certain value of η but beyond this point it decreases. This is due to the revised nanoparticle concentration boundary condition.

5. Conclusion

In this paper, we have studied the combined effects of Soret and Dufour numbers on the fluid flow, heat and mass transfer of a Casson nanofluid over an unsteady stretching sheet in the presence of thermal radiation and heat generation. The effects of partial slip on the velocity boundary condition, convective thermal boundary condition, Brownian and thermophoresis diffusion coefficients on the concentration boundary condition

are also analyzed here. The governing equations were solved using the Spectral Relaxation Method. The study has shown, inter alia, that by increasing the Casson, Dufour and unsteadiness parameters, we reduce the fluid velocity, temperature and concentration profiles. As would be expected, increasing thermal radiation increases the temperature profiles and also the Soret parameter increases the concentration profiles. As has been shown previously in the literature for Newtonian fluids, our findings are that for a Casson nanofluid as discussed in this paper, increasing the intensity of the magnetic field has the effect of reducing the fluid flow while enhancing the fluid temperature. Additional conclusions that can be drawn from this study are that;

- Increasing the velocity slip parameter reduces the velocity profile.
- Increasing the heat generation parameter reduces the temperature profile.

Acknowledgement

The authors are thankful to the University of KwaZulu-Natal and Claude Leon Foundation, South Africa for the necessary support.

References

[1] S. Choi, Enhancing thermal conductivity of fluids with nanoparticles, ASME-Publ. Fed. 231 (1995) 99–106.
[2] J. Buongiorno, Convective transport in nanofluids, J. Heat Trans. 128 (2006) 240–250.
[3] A. Noghrehabadi, R. Pourrajab, M. Ghalambaz, Effect of partial slip boundary condition on the flow and heat transfer of nanofluids past stretching sheet prescribed constant wall temperature, Int. J. Ther. Sci. 54 (2012) 253–261.
[4] W.A. Khan, I. Pop, Boundary layer flow of a nanofluid past a stretching sheet, Int. J. Heat Mass Trans 53 (2010) 2477–2483.
[5] S. Nadeem, R.U. Haq, N.S. Akbar, C. Lee, Z.H. Khan, Numerical study of boundary layer flow and heat transfer of Oldroyd-B nanofluid towards a stretching sheet, PLoS One 8 (2013) e6981, http://dx.doi.org/10.1371/journal.pone.0069811.
[6] O.D. Makinde, W.A. Khan, Z.H. Khan, Buoyancy effects on MHD stagnation point flow and heat transfer of a nanofluid past a convectively heated stretching/shrinking sheet, Int. J. Heat Mass Trans. 62 (2013) 526–533.
[7] N.A. Haroun, P. Sibanda, S. Mondal, S.S. Motsa, On unsteady MHD mixed convection in a nanofluid due to a stretching/shrinking surface with suction/injection using the spectral relaxation method, Bound. Val. Probl. 1 (2015) 1–17, http://dx.doi.org/10.1186/s13661-015-0289-5.
[8] N.A. Haroun, P. Sibanda, S. Mondal, S.S. Motsa, M.M. Rashidi, Heat and mass transfer of nanofluid through an impulsively vertical stretching surface using the spectral relaxation method, Bound. Value Problems 161 (2015) 1–16, http://dx.doi.org/10.1186/s13661-015-0424-3.
[9] M. Mustafa, T. Hayat, I. Pop, A. Hendi, Stagnation-point flow and heat transfer of a Casson fluid towards a stretching sheet, Z. Naturforsch. 67a (2011) 70–76.
[10] M. Mustafa, T. Hayat, I. Pop, A. Aziz, Unsteady boundary layer flow of a Casson fluid due to an impulsively started moving flat plate, Heat Trans.-As. Res. 40 (2011) 563–576.
[11] S.K. Nandy, Analytical solution of MHD stagnation-point flow and heat transfer of Casson fluid over a stretching sheet with partial slip, ISRN Therm. (2013), http://dx.doi.org/10.1155/2013/108264. Article ID 108264.
[12] G. Makanda, S. Shaw, P. Sibanda, Diffusion of chemically reactive species in Casson fluid flow over an Unsteady Stretching surface in porous medium in the presence of a magnetic field, Math. Probl. Eng. 2015 (2015), http://dx.doi.org/10.1155/2015/724596, 10 pages Article ID 724596.
[13] K. Bhattacharyya, MHD stagnation-point flow of Casson fluid and heat transfer over a stretching sheet with thermal radiation, J. Therm. (2013), http://dx.doi.org/10.1155/2013/169674. Article ID 169674.
[14] S. Mukhopadhyay, P.R. De, K. Bhattacharyya, G.C. Layek, Casson fluid flow over an unsteady stretching surface, Ain Shams Eng. J. 4 (2013) 933–938.
[15] H.I. Andersson, J.B. Aarseth, B.S. Dandapat, Heat transfer in a liquid film on an unsteady stretching surface, Int. J. Heat Mass Trans. 43 (2000) 69–74.
[16] T. Hayat, S.A. Shehzad, A. Alsaedi, Soret and Dufour effects on magnetohydrodynamic(MHD) flow of Casson fluid, Appl. Math. Mech. – Engl Ed. 33 (2012) 1301–1312.
[17] S. Nadeem, R.U. Haq, N.S. Akbar, Z.H. Khan, MHD three-dimensional Casson fluid flow past a porous linearly stretching sheet, Alexan. Eng. J. 52 (2012) 577–582.
[18] K. Bhattacharyya, T. Hayat, A. Alsaedi, Analytic solution for magnetohydrodynamic boundary layer flow of Casson fluid over a stretching/shrinking sheet with wall mass transfer, Chin. Phys. B 22 (2013) 0247021–0247026.
[19] S. Nadeem, R.U. Haq, C. Lee, MHD flow of a Casson fluid over an exponentially shrinking sheet, Sci. Iranic. 19 (2012) 1550–1553.
[20] S. Nadeem, R.U. Haq, N.S. Akbar, MHD three-dimensional boundary layer flow of Casson nanofluid past a linearly stretching sheet with convective boundary condition, IEEE Trans. Nanotech. 13 (2014) 109–115.
[21] S. Mukhopadhyay, Effects of thermal radiation on Casson fluid flow and heat transfer over an unsteady stretching surface subjected to suction/blowing, Chin. Phys. B 22 (2013) 114702.
[22] C.S.K. Raju, N. Sandeep, V. Sugunamma, M.B. Jayachandra, R.J.V. Ramana, Heat and mass transfer in magnetohydrodynamic Casson fluid over an exponentially permeable stretching surface, Eng. Sci. Technol. Int. J., in press. doi: http://dx.doi.org/10.1016/j.jestch.2015.05.010.
[23] A.V. Kunetsov, D.A. Nield, Natural convective boundary layer flow of a nanofluid past a vertical plate: a revised model, Int. J. Ther. Sci. 77 (2014) 126–129.
[24] S.S. Motsa, A new spectral relaxation method for similarity variable nonlinear boundary layer flow systems, Chem. Eng. Commun. 201 (2014) 241–256.
[25] S.S. Motsa, P.G. Dlamini, M. Khumalo, Spectral relaxation method and spectral quasilinearization method for solving unsteady boundary layer flow problems, Adv. Math. Phys. 2014 (2014), http://dx.doi.org/10.1155/2014/341964. Article ID 341964.
[26] S.S. Motsa, Z.G. Makukula, On spectral relaxation method approach for steady von Karman flow of a Reiner–Rivlin fluid with Joule heating and viscous dissipation, Cen. Eur. J. Phys. 11 (2013) 363–374.
[27] M. Nakamura, T. Sawada, Numerical Study on the flow of a non-Newtonian fluid through an axisymmetric stenosis, J. Biomech. Eng. 110 (1988) 137–143.
[28] S. Sharidan, T. Mahmood, I. Pop, Similarity solutions for the unsteady boundary layer flow and heat transfer due to a stretching sheet, Int. J. Appl. Mech. Eng. 11 (2006) 647–654.
[29] A.J. Chamkha, A.M. Aly, M.A. Mansour, Similarity solution for unsteady heat and mass transfer from a stretching surface embedded in a porous medium with suction/injection and chemical reaction effects, Chem. Eng. Commun. 197 (2010) 846–858.
[30] T.R. Mahapatra, A.S. Gupta, Heat transfer in stagnation-point flow towards a stretching sheet, Heat Mass Trans. 38 (2002) 517–521.

[31] A. Ishak, R. Nazar, N.M. Arifin, I. Pop, Mixed convection of the stagnation-point flow towards a stretching vertical permeable sheet, Malay. J. Math. Sci. 1 (2007) 217–226.
[32] B. Sahoo, Y. Do, Effects of slip on sheet-driven flow and heat transfer of a third grade fluid past a stretching sheet, Int. Commun. Heat Mass Trans. 37 (2010) 1064–1071.
[33] O.A. Beg, V.R. Prasad, B. Vasu, N.B. Reddy, Q. Li, R. Bhargava, Free convection heat and mass transfer from an isothermal sphere to a micropolar regime with Soret/Dufour effects, Int. J. Heat Mass Trans. 54 (2011) 9–18.
[34] F. Mabood, S.M. Ibrahim, M.M. Rashidi, M.S. Shadloo, Giulio Lorenzini, Non-uniform heat source/sink and Soret effects on MHD non-Darcian convective flow past a stretching sheet in a Micropolar fluid with radiation, Int. J. Heat Mass Trans. 93 (2016) 674–682.